Optimizing the lattice design of a diffraction-limited storage ring with a rational combination of particle swarm and genetic algorithms *

Yi Jiao(焦毅)[1)] Gang Xu(徐刚)

Key Laboratory of Particle Acceleration Physics and Technology, Institute of High Energy Physics, Chinese Academy of Sciences, Beijing 100049, China

Abstract: In the lattice design of a diffraction-limited storage ring (DLSR) consisting of compact multi-bend achromats (MBAs), it is challenging to simultaneously achieve an ultralow emittance and a satisfactory nonlinear performance, due to extremely large nonlinearities and limited tuning ranges of the element parameters. Nevertheless, in this paper we show that the potential of a DLSR design can be explored with a successive and iterative implementation of the multi-objective particle swarm optimization (MOPSO) and multi-objective genetic algorithm (MOGA). For the High Energy Photon Source, a planned kilometer-scale DLSR, optimizations indicate that it is feasible to attain a natural emittance of about 50 pm·rad, and simultaneously realize a sufficient ring acceptance for on-axis longitudinal injection, by using a hybrid MBA lattice. In particular, this study demonstrates that a rational combination of the MOPSO and MOGA is more effective than either of them alone, in approaching the true global optima of an explorative multi-objective problem with many optimizing variables and local optima.

Keywords: diffraction-limited storage ring, High Energy Photon Source, multi-objective particle swarm optimization, multi-objective genetic algorithm, lattice design

PACS: 29.20.db, 41.85.-p **DOI:** 10.1088/1674-1137/41/2/027001

1 Introduction

In the past few decades, third generation light sources (TGLSs), based on electron storage rings with natural emittances of the order of a few nm.rad, have become one of the most widely used platforms providing high quality photon beam for fundamental research in physics, chemistry, materials science, biology and medicine [1]. Nevertheless, there is an unceasing pursuit of better sources. Early in the 1990s, it was proposed [2] to use multi-bend achromat (MBA) lattices to reduce the natural emittance by at least one order of magnitude to approach the diffraction limit for photons in the energy range of interest (especially in the X-ray range) for the user community, so as to push beyond the brightness and coherence available in TGLSs. These new-generation light sources, usually called diffraction-limited storage rings (DLSRs) [3], have only recently become practical and cost effective, with the development of small-aperture magnet and vacuum systems [4–5] and progress in beam dynamics issues. Due to the predicted superior performance of DLSRs over TGLSs, many laboratories are now constructing storage ring light sources with natural emittance of a few hundred pm·rad (e.g., MAX-IV [6] and Sirius [7]), and seriously considering upgrading existing machines to DLSRs or building new green-field MBA light sources.

A standard MBA typically has several identical unit cells in the middle and one matching cell on each side, providing a dispersion-free drift space of a few meters to accommodate the insertion devices (IDs) dedicated to the emission of high-flux photon beam. To attain an ultralow emittance with a compact layout, it is common [8] to use combined-function dipoles and strong quadrupoles to achieve small optical parameters in the dipoles that are close to the theoretical minimum emittance (TME [9]) conditions. In some standard-MBA designs [e.g., 10, 11] the emittance is further reduced with damping wigglers. To correct the large natural chromaticities arising from the strong focusing, sextupoles are usually located in all the unit cells. Even so, it was found [12] that the sextupole strengths scale approximately inversely linearly with the natural emittance. Experience [13] indicates that if the natural emittance is reduced to a few tens of pm·rad with standard MBAs, impractically high sextupole gradients or very thick sextupoles (e.g., thicker than quadrupoles) will be needed, leading to an undesirable DLSR design.

To make a more effective chromatic correction, a particular MBA concept, called the 'hybrid MBA', has been

Received 26 July 2016

* Supported by NSFC (11475202, 11405187) and Youth Innovation Promotion Association CAS (2015009)

1) E-mail: jiaoyi@ihep.ac.cn

proposed [14]. Taking a hybrid 7BA as an example (see Fig. 1), the four outer dipoles are used to create two dispersion bumps with much larger dispersions than available in a standard MBA, and all the chromatic sextupoles are placed therein. In this way, the sextupole strengths can be reduced to an achievable level with conventional magnet technology. The price of doing so is that the optical functions in the four outer dipoles are not optimized for emittance minimization. To compensate for this side effect, longitudinal gradients are introduced to the outer dipoles and even stronger focusing than in a standard MBA is adopted neighboring the inner three dipoles, to keep the natural emittance at an ultralow level. Moreover, the linear optics is matched such that a $-\boldsymbol{I}$ transportation is made between each pair of sextupoles, so as to cancel most of the nonlinearities induced by the sextupoles. Due to these advantages, the hybrid MBA lattice has been adopted in many projects, e.g., ESRF-II [14] and APS-U [15].

A kilometre-scale storage ring light source with a beam energy of 5 to 6 GeV, named the High Energy Photon Source (HEPS), has been proposed for a long time and is to be built in the near future. The lattice design has been continuously evolved. Recently a hybrid 7BA design with a natural emittance of 60.1 pm·rad at 6 GeV was developed for the HEPS [16]. This design (denoted as 'mode I' hereafter) consists of 48 identical hybrid 7BAs and has a circumference of 1296.6 m. Each 7BA is of about 27 m, with a 6-m ID section. The layout is very compact. Several gaps between adjacent magnets (D3, D4 and D8 in Fig. 1) are of only 7.5 cm. And, to reserve as much space as possible for diagnostics and other equipment, in each 7BA only six sextupoles and two octupoles are used and located in the dispersion bumps for chromatic correction and nonlinear optimization. The layout and optical functions of a 7BA are shown in Fig. 1, and the main parameters of the ring are listed in Table 1.

To evaluate the nonlinear performance of a 'realistic' machine, it is necessary to consider various errors (such as misalignments, rotations, strength errors, etc.) in the lattice evaluation. One needs to generate a large number of random seeds for errors, add them to the bare lattice, simulate the lattice calibration procedure, and finally calculate the ring acceptance, such as the dynamic aperture (DA) and momentum acceptance (MA). Such a process is, however, very complex and time-consuming. Instead, in the HEPS design we used the 'effective' DA and MA of the bare lattice as indicators of the nonlinear performance. Within the effective DA or MA, it is

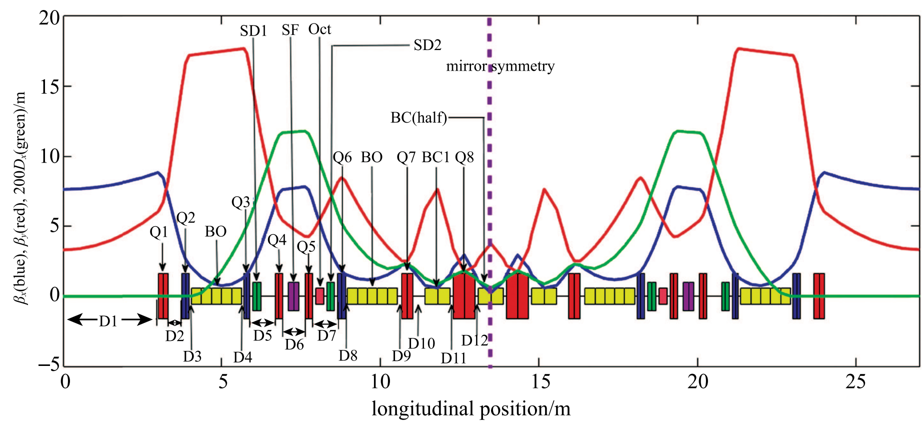

Fig. 1. (color online) Optical functions and layout of a hybrid 7BA of the HEPS 'mode I' design. Due to the mirror symmetry, only the elements on the left side of the 7BA are labelled.

Table 1. Main parameters of the original and optimized HEPS designs.

	mode I	mode II	mode III	mode IV	mode V
working point (H/V)	113.20/41.28	116.16/41.12	111.28/41.11	112.13/41.18	112.23/39.14
natural chromaticity (H/V)	−149/−128	−214/−133	−134/−136	−140/−137	−140/−126
beta functions in ID section (H/V)/m	7.6/3.3	9/3.2	7/3.1	8.0/3.1	7.9/4.2
natural emittance ε_0/(pm·rad)	60.1	59.4	58.9	55.8	52.1
lengths of (SD/SF/OF)/m	0.25/0.34/0.26	0.25/0.34/0.26	0.22/0.25/0.2	0.22/0.25/0.2	0.22/0.25/0.2
K_s/K_{oct} w/0.2-m multipoles/ (m^{-3} /m^{-4})	294/3.3×10^4	255/1.5× 10^4	273/1.3×10^4	273/1.4× 10^4	284/1.3×10^4
momentum acceptance	2.4%	3%	3.6%	3.6%	3.5%
horizontal and vertical DA size/mm	2.5/2.2	2.5/3.5	3.0/4.4	3.5/4.5	3.0/4.8

required that not only the motion remains stable after tracking over a few thousand turns, but also the tune footprint is bounded by the integer and half integer resonances nearest to the working point (see Fig. 2). The reasoning behind this definition is that the integer resonances can be excited by even small field imperfections, and are generally fatal to beam dynamics. In TGLSs it may be possible to approach or even cross the half integer resonances without beam loss [see, e.g., 17], with the state-of-art optics correction technique. But in a DLSR, since the linear optics is generally pushed to its extreme, the nonlinear dynamics is more sensitive to machine imperfections. Detailed simulation studies for the HEPS design [18] indicate that to avoid particle loss due to crossing of half integer resonances, the rms beta beats should be kept to a sufficiently small level. Thus, the authors think that the effective DA and MA can provide a quick, somewhat conservative but reasonable measure of the 'realistic' ring acceptance of a DLSR in many cases, especially with only the bare lattice in hand.

For the HEPS 'mode I' design, the multipoles were grouped in four families (SD1, SD2, SF and Oct). Two sextupole families were for chromatic correction, and only two free knobs were left for DA and MA optimization. This, however, enabled us to globally scan the multipole strengths in a reasonable computing time, based on numerical tracking with the AT [19] program and frequency map analysis [20]. Unfortunately, it was found difficult to simultaneously optimize the effective DA and MA. The compromise solution predicts an effective DA of 2.5 (or 2.2) mm in the x (or y) plane and an effective MA of 2.4%, with the results shown in Figs. 2 and 3.

To resolve the difficulty for injection due to small DA, a novel on-axis longitudinal injection scheme enabled by phase manipulation of a double-frequency RF system was proposed [21]. Compared with the scheme with a single-frequency RF system [22], this scheme can greatly reduce the requirement of the MA to about 3%. We believe that it is possible, although challenging, to reach such a target on MA. Actually, by means of sextupole strength minimization and tune space scan for the same layout as the 'mode I' design, we attained a better design [23] (denoted as 'mode II' hereafter) with a similar emittance, 59.4 pm·rad, but larger effective MA (~3%)

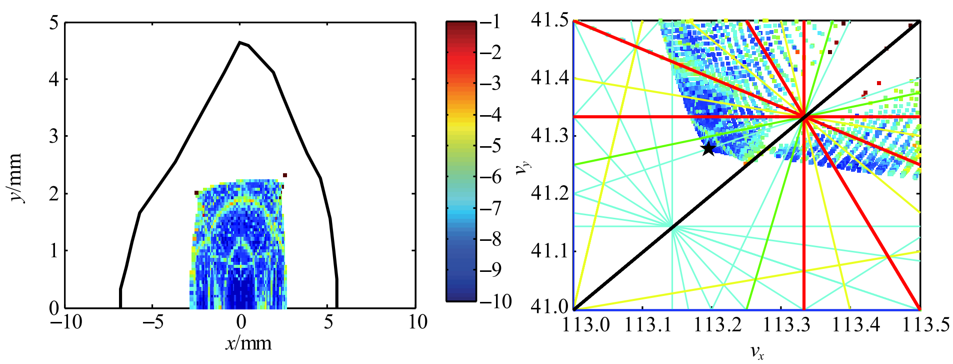

Fig. 2. (color online) Effective DA and the corresponding frequency map for the HEPS 'mode I' design. The DA, with all surviving particles after tracking over 1000 turns, is also plotted (black curve) for comparison. In this figure and Figs. 3, 11 and 12 below, the colors, from blue to red, represent the stabilities of the particle motion, from regular to irregular; the black star represents the working point; and the bare lattice was used in the DA and MA tracking.

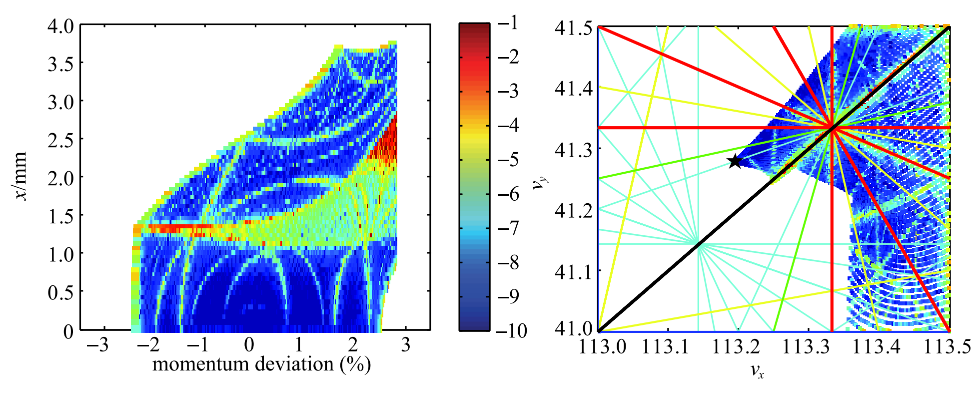

Fig. 3. (color online) Effective MA and the corresponding frequency map for the HEPS 'mode I' design.

and DA (~2.5 mm in x and 3.5 mm in y plane). The main parameters of the 'mode II' design are also listed in Table 1.

Nevertheless, before taking the 'mode II' lattice as the HEPS 'final design', it is necessary and important to globally scan all the tunable element parameters (while keeping the circumference basically unchanged, i.e., varied in +/− 1 m) to explore the ultimate performance of such a hybrid 7BA design. The performance parameters include the achievable minimum natural emittance and the maximum ring acceptance at a specific natural emittance. It is also interesting to investigate the dependence of the nonlinear performance on various linear optical parameters.

For a hybrid 7BA, there are more than 20 tunable element parameters. A global grid scan may take too long a time to exhaust all the possibilities. In contrast, a more efficient way is to use stochastic optimization algorithms, e.g., the multi-objective genetic algorithm (MOGA) and multi-objective particle swarm optimization (MOPSO). The MOGA methods mimic the process of natural selection and evolution of species, and have been widely applied to many accelerator optimization problems [24–28]. MOPSO, on the other hand, emulates the self-organizing behavior of social animal living in group, and has been recently used to optimize linac operation and ring dynamics [29–31].

It has been demonstrated that both algorithms are powerful and effective in solving problems with piecewise continuous and highly nonlinear objectives and many local optima. Nevertheless, a recent study [31] showed that MOPSO converges faster than MOGA, and is not as dependent on the distribution of initial population as MOGA. To test this, we compared the performance of these two algorithms by applying them to a problem whose answer was known. The results are presented in Section 2. It was found that each algorithm has its own unique advantage, and implementing them in a successive and iterative way will be more effective than using either of them alone in approaching the true global optima for an explorative multi-objective problem. As will be shown in Section 3, with such a combination of MOPSO and MOGA, we were able to find solutions showing optimal trade-offs between the natural emittance and ring acceptance for the HEPS hybrid 7BA design. Conclusions will be given in Section 4.

2 Optimization of the natural emittance and chromatic sextupole strengths

2.1 Optimization for the case with a fixed ID section length

Experience [23] indicates that sextupole strength minimization followed by tune space scan is an effective way to improve the nonlinear performance. Thus, we first looked at the trade-offs between the natural emittance and the sextupole strengths required for chromatic correction, for the case with a fixed ID section length, $L_{\mathrm{ID}} \equiv 6$ m. Since the evaluation limits itself in the linear optics regime and is very fast (less than 1 s per evaluation), we could obtain optimal solutions in a much shorter time than that it takes to directly optimize the effective DA and MA.

One of the MOGA methods, the non-dominated sorting genetic algorithm II (NSGA-II [32]), was used in the optimization. Twenty-six element parameters were used as optimizing variables, and varied within specific ranges that are determined by practical or optical constraints (see Table 2 for details). Two objective functions, weighted natural emittance ε_0 and weighted chromatic sextupole strengths, were defined. For ease of comparison of the sextupole strengths between different solutions, the sextupoles were grouped in just two families (SD, SF) with identical lengths of 0.2 m, such that for specific corrected chromaticities ([0.5, 0.5] in this study) there is a unique solution of the sextupole strengths (K_{sd}, K_{sf}), which were then represented with a nominal strength,

$$K_{\mathrm{s}} = \sqrt{(K_{\mathrm{sf}}^2 + K_{\mathrm{sd}}^2)/2}. \tag{1}$$

To ensure enough diversity in the initial population, we first randomly generated lots of possible combinations of optimizing variables with large fluctuations around those of the 'mode I' and 'mode II' designs, from which we selected 6000 solutions with stable optics and used them as the initial population. This took a long, but still acceptable, computing time.

Table 2. Optimizing variables and scanning range in the optimization.

variables	scanning range
lengths of drifts	[0.1, 1.6] m
gradients of (Q1 to Q6)	[−2.6, 2.6] m^{-2}
gradients of (Q7 and Q8)	[−4, 4] m^{-2}
gradients of dipoles (BC1 and BC2)	[−2.4, 2.4] m^{-2}
length of inner dipoles	[0.6, 1.0] m
length of outer dipoles	[1.2, 1.8] m
dipole angles	[0.1, 2] degree

For each ensemble of variables, before evaluating the ε_0 and K_{s}, several quadrupoles were tuned to match (if feasible) the achromatic condition (with K_{Q3} and K_{Q4}) and realize the $-\boldsymbol{I}$ transportation between each pair of the sextupoles, SFs (with K_{Q5}, K_{Q6} and K_{Q7}). Moreover, to ensure that the obtained solutions have desirable optics, as many constraints as possible were considered:

(1) a reasonable maximum value of beta function along the ring, $\max(\beta_{x,y}) \leqslant 30$ m,

(2) reasonably low beta functions in ID section for high brightness, 1.5 m $\leqslant \beta_y <$ 4 m and 1.5 m $\leqslant \beta_x <$ 15 m,

(3) stability of the optics, $\mathrm{Tr}(M_{x,y}) < 2$, with $M_{x,y}$ being the transfer matrix of the ring in the x or y plane,

(4) fractional tunes in (0, 0.5), which is favorable against the resistive wall instability,

(5) reasonable natural chromaticities, $|\xi_{x,y}| \leqslant 5.5$ in one 7BA,

(6) all drifts between adjacent magnets longer than 0.1 m,

(7) one of the drifts (D10, D11 and D12) longer than 0.35 m to accommodate a three-pole wiggler, which is to be used as a hard X-ray source,

(8) and reasonably low energy loss in each turn due to synchrotron radiation ($U_0 \leqslant$ 2.2 MeV).

The degree of the violation of each constraint was measured with a weight factor. If a specific constraint is satisfied, the corresponding weight factor will be one; otherwise the factor will be assigned a value of more than 1. And, the more violated the constraint is, the larger the factor will be. These factors were then multiplied by the calculated ε_0 and K_s to get the values of the two objective functions. In this way, even with similar or the same ε_0 and K_s, the desirable solutions (meet all constraints) will have smaller objective functions than those that violate certain constraints, and will be assigned a higher rank with the non-dominated sorting, and have higher priorities for survival and reproduction in the evolution chain.

It is worth mentioning that in the optimization only the quadrupole gradients, rather than both the gradients and lengths, were used as optimizing variables. This is based on the consideration that for a specific change in the transverse focusing, there will be a myriad of possible combinations of the quadrupole lengths and gradients, whereas we are just interested in the solutions which have the shortest possible quadrupoles. If both the quadrupole lengths and gradients are varied in the optimization, it probably requires an additional sorting of the solutions, and needs to evolve a larger population over more generations.

Instead, we optimized the quadrupole lengths with an iteration of the MOGA algorithm. In the first MOGA evolution, quadrupoles had the same lengths as in the 'mode I' design, while their gradients were varied in larger ranges than available. According to the covering range of gradients of the final population, we adjusted the quadrupole lengths in such a way that all the gradients are below but close to their upper limits. And then, the final population of the first MOGA (with small modifications on gradients, if necessary) was used as the initial population of a new MOGA evolution, where the quadrupoles had modified lengths and their gradients were varied within the available ranges this time. The population evolved over 1000 generations, and the population was already very close to the final population at generation 600, as shown in Fig. 4. One can see that for the HEPS hybrid 7BA design, it is feasible to reduce the natural emittance to about 43.5 pm·rad, or to decrease the nominal sextupole strength K_s to about 180 m^{-3} at ε_0 = 60 pm·rad, which is much smaller than those in the 'mode I' and 'mode II' designs (294 and 255 m^{-3} if with 0.2-m sextupoles).

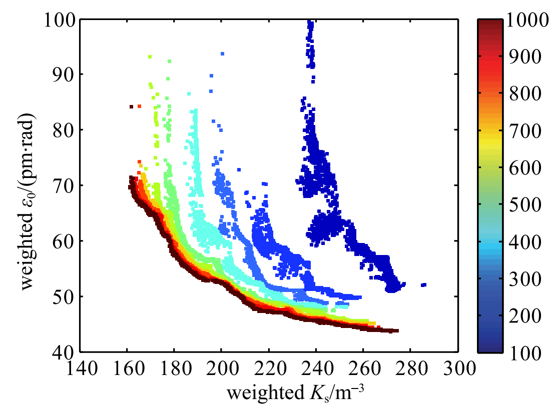

Fig. 4. (color online) Objective functions of the population at every 100th generation (in different color) with MOGA.

Among the solutions of the 600th to 1000th generation, we kept only the desirable solutions with ε_0 below 65 pm·rad, and then re-evaluated them to get other optical parameters, including the beta functions at the ID section, dispersion at the dispersion bump (D_x), tunes and natural chromaticities. The distributions of these solutions in different sub-parameter planes are shown in Fig. 5.

In these solutions, the nominal sextupole strength K_s decreases monotonically with increasing ε_0 and increasing D_x. Besides, many optical parameters rely heavily on the integer tunes, especially the horizontal one. For instances, different integer tune regions correspond to different covering ranges of the beta functions at the ID section. And, a larger horizontal integer tune corresponds to larger natural chromaticities, a larger dispersion at the dispersion bump, a larger natural emittance and weaker sextupoles. Although the sextupole strength is associated with both the dispersion at the dispersion bump and the natural chromaticities, apparently, it is more related to the former factor. Further study revealed that to achieve a larger D_x, one needs to match the optics in such a way that the optical functions in the four outer dipoles are more deviated from the TME conditions, leading to an increase in emittance. To keep the emittance at an ultralow level, stronger focusing (a larger horizontal tune) is needed to squeeze the optical functions in the inner three dipoles and get them closer

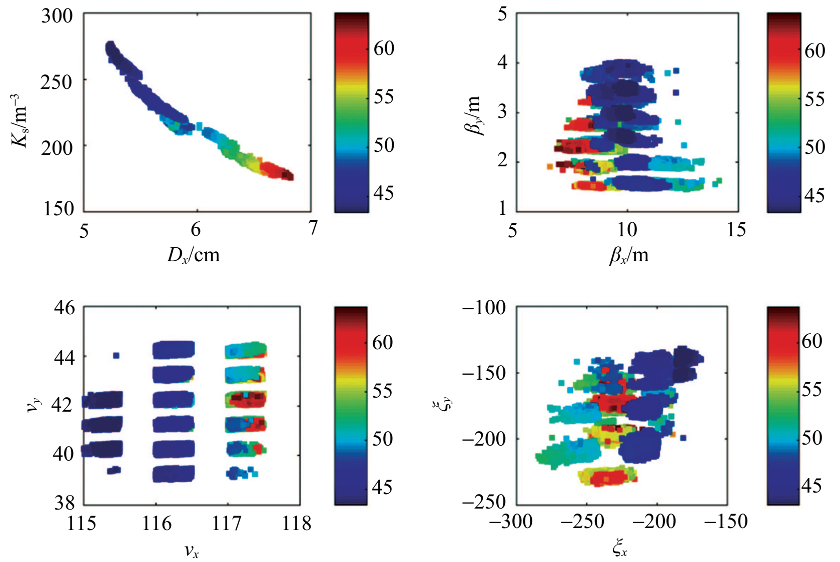

Fig. 5. (color online) Selected MOGA solutions projected onto the K_s-D_x, β_x-β_y, υ_x-υ_y and ξ_x-ξ_y planes. The colors represent the values of the natural emittance (in unit of pm·rad).

to the TME conditions. Therefore choosing a larger horizontal integer tune helps to reach a balance between the ultralow emittance and weakest possible sextupoles.

2.2 Optimization for the case with a variable ID section length

In the above optimization, the ID section length was fixed to 6 m. One can consider that if $L_{\rm ID}$ is smaller, the variables for the position and length of magnets will have larger adjustment space, and it will be feasible to achieve designs with better performance.

To explore the potential of the design with a shorter ID section length, in this optimization the $L_{\rm ID}$ was also used as an optimizing variable, and varied in the range of [5, 7] m. The final population of MOGA obtained in Section 2.1, with small modifications, was used as the initial population of this optimization. The modifications included generating random values drawn from a normal distribution with an average of 6 m for the $L_{\rm ID}$, and accordingly adjusting the length of the drift D6 to keep the circumference unchanged. To ensure that most of the individuals in the initial population have stable optics, the standard deviation of the random seeds for $L_{\rm ID}$ was, however, set to a small value, 0.1 m.

For comparison, the same initial population was evolved over 800 generations with MOGA and MOPSO, respectively. The parameter settings of these two algorithms are the same as described in Ref. [31]. It was found that the solutions with $L_{\rm ID}$ larger than 6 m were gradually phased out in the evolution with both algorithms. In addition, as shown in Fig. 6, most of the solutions at the last generation of MOGA and MOPSO have better performance (e.g., with smaller K_s at a specific ε_0) than those optimized for $L_{\rm ID} \equiv 6$ m.

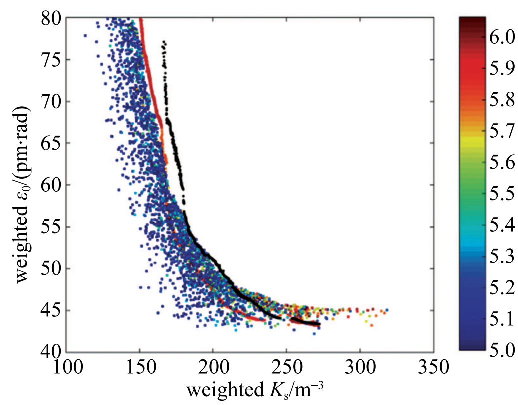

Fig. 6. (color online) MOGA solutions for fixed ID section length, $L_{\rm ID} \equiv 6$ m (black curve), and the solutions with MOPSO (sparsely distributed dots) and MOGA (narrowly distributed dots) for a variable $L_{\rm ID}$, with the colors representing the $L_{\rm ID}$ values (in unit of m).

On the other hand, the difference in the performance of these two algorithms is also obvious. For MOGA, the $L_{\rm ID}$ values of the final population do not exceed the $L_{\rm ID}$ covering range of the initial population, with a minimum of about 5.75 m. For MOPSO, a majority of solutions have $L_{\rm ID}$ values close to 5 m, and in particular, promise smaller K_s than those obtained with MOGA. This difference has been explained in Ref. [31]. In MOPSO, each surviving individual adjusts its moving pace and direction in parameter space at every iterative step, according to its own historical experience and relative position within the population. The new solutions are not generated from the existing good solutions, as is done in

MOGA. Thus, MOPSO intrinsically allows more diversity than MOGA, and does not need a diverse seeding in the initial population.

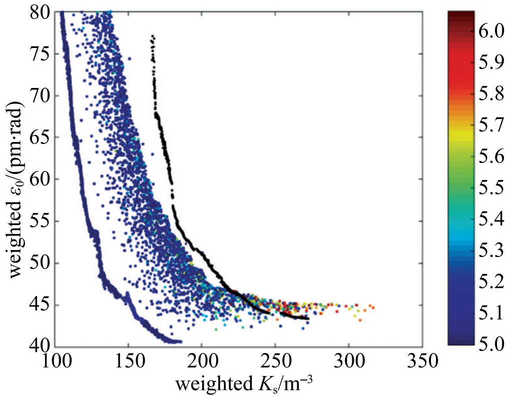

Fig. 7. (color online) MOGA solutions for fixed ID section length, $L_{\mathrm{ID}} \equiv 6$ m (black curve), and the solutions for variable L_{ID} after evolution of 500 more generations with MOPSO (sparsely distributed dots) and MOGA (narrowly distributed dots) for a variable L_{ID}, with the colors representing the L_{ID} values (in unit of m).

Nevertheless, one can see from Fig. 6 that the final solutions of MOPSO are distributed rather sparsely in the objective function space. Also, in the low emittance region ($\varepsilon_0 \sim 45$ pm·rad), some solutions still have L_{ID} values close to 6 m, with even larger K_{s} than those optimized for $L_{\mathrm{ID}} \equiv 6$ m. As shown in Fig. 7, the situation does not substantially change even after 500 more generations of evolution with MOPSO. Just for comparison, based on the MOPSO population at generation 800, we implemented MOGA for 500 generations. One can see from Fig. 7 that the final population of MOGA reached a better convergence, having solutions with all L_{ID} values close to 5 m and with superior performance over those optimized for $L_{\mathrm{ID}} \equiv 6$ m in the whole emittance range of interest.

By optimizing the design first with MOPSO and then with MOGA, we obtained solutions that agree with expectations. The results suggest that by shortening the ID section from 6 m to about 5 m, the natural emittance can be further reduced to about 40 pm·rad, or the nominal sextupole strength K_{s} can be further decreased by at least 40% at $\varepsilon_0 = 60$ pm·rad. On the other hand, a shorter L_{ID} implies a reduced space for IDs, which may affect the performance of the light source. Therefore in the following we will only discuss the case with $L_{\mathrm{ID}} \equiv$ 6 m.

From the above results one can learn that MOGA depends significantly on the distribution of the initial population. If there is not enough diversity in the initial population, MOGA may converge to local optima rather than the true global optima. Worse still, the MOGA itself cannot give a measure of the diversity of a population. Consequently, if applying MOGA to a typical exploratory multi-objective problem with many optimizing variables and local optima, and without another effective algorithm (e.g., MOPSO in this study) for comparison, one cannot know for sure whether the final solutions reveal optimal trade-offs between the different objectives. In short, to make an effective MOGA optimization, it is critical, and also challenging, to seed the initial population with high enough diversity. Fortunately, as demonstrated above, this difficulty can be overcome with the MOPSO, which has an intrinsic ability to breed more diversity in the evolution of the population. Once the diversity of solutions is ensured, MOGA can reach a better convergence than MOPSO to the true global optima. Therefore, evolving the population with a rational combination of MOPSO and MOGA would be more effective than using either of these two algorithms alone.

3 Optimization of the natural emittance and ring acceptance

3.1 Nonlinear performance of the solutions with minimized sextupole strengths

In Section 2.1, we obtained solutions showing optimal trade-offs between the natural emittance ε_0 and the chromatic sextupole strengths (represented with a nominal strength K_{s}) for the case with $L_{\mathrm{ID}} \equiv 6$ m.

The corresponding nonlinear performance of these solutions was then evaluated. For simplicity, the nonlinear performance was measured with the scaled DA area (in unit of mm^2), i.e., the product of the horizontal and vertical effective DA sizes normalized with respect to the square root of the values of beta functions at the start point of DA tracking. Among the solutions with the same or very similar tunes, the one with the lowest K_{s} was selected for the subsequent DA and MA optimization, where the multipoles were split into four families again and their strengths were scanned with small step sizes (5 m^{-3} for sextupoles and 100 m^{-4} for octupoles). The available scaled DA area for a specific set of tunes was obtained through numerical tracking for the multipolar set (if exist) that results in an effective MA of not less than 3% and the largest scaled DA area.

To look at the relations between the scaled DA area and other parameters, such as ε_0, K_{s} and the tunes, the solutions were separated into six parts, as shown in Fig. 8(a). In each part, the solutions covered a large tune area, and the available maximum scaled DA area was obtained by comparing those with different tunes. The results are shown in Fig. 8(b). It appears feasible to find solutions with scaled DA area larger than that of the 'mode II' design (1.63 mm^2), and with ε_0 below 60 pm·rad and effective MA equal to or above 3%. Nevertheless, Figure 8(b) does not show a monotonic variation of the scaled DA area with ε_0 as for the K_s. The available scaled DA area also depends on the horizontal integer tunes. This suggests that the sextupole strength minimization followed by tune space scan may be not the best way to find the optimal trade-offs between the natural emittance and ring acceptance. It is necessary to include the multipole strengths in the global optimization. Nevertheless, these obtained solutions provide a good starting point for the new optimization, which uses the natural emittance and ring acceptance directly as optimizing objectives.

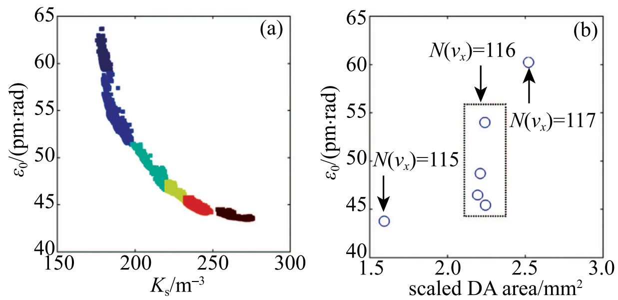

Fig. 8. (color online) Solutions projected onto the K_s-ε_0 plane, and the available maximum scaled DA area at different emittance range.

3.2 Direct optimization of the natural emittance and ring acceptance

In this optimization, the multipole strengths were also used as optimizing variables. The upper limit of the sextupole strength was set to 280 m^{-3}, by assuming a larger pole radius for the sextupoles (14 mm) than quadrupoles (12.5 mm), for the ease of extracting the photon beam from the upstream IDs. The multipoles were split into eight families to provide six free knobs for nonlinear optimization. The nonlinear performance, this time, was measured with the scaled ring acceptance (in unit of mm^2), i.e., the product of the scaled DA area and the effective MA (normalized with respect to 3%). Thirty-two optimizing variables (all tunable element parameters except L_{ID}) and two objective functions (weighted natural emittance and scaled ring acceptance) were used.

The individuals of the initial population were selected from the solutions obtained in Section 3.1 that promise a larger scaled DA area than the 'mode II' design. Although the objective evaluation in this case took a much longer time (~60 s per evaluation) than for the evaluation just in the linear optics regime, we chose a relatively large population size of 4000 to ensure the comprehensiveness of the solutions.

In addition, to guarantee the surviving solutions have robust nonlinear performance, more constraints were considered. The effective DA or MA, this time, was determined by the amplitude or momentum deviation with tunes first approaching the integer resonances by 0.05 or the half integer resonances by 0.01. In addition, it was noticed that the space charge effect can cause a maximum vertical tune shift of about 0.01 for HEPS with a beam current of 200 mA [33]. To avoid particles being trapped by coupling resonances due to the space charge effect, it is required that within the effective MA, the fractional tunes for any momentum deviation should be separated by at least 0.015.

The sextupole lengths were optimized by iterative implementations of MOPSO and MOGA, similar to what was done for optimizing the quadrupole lengths. During the iterations, we also gradually reduced the emittance range of interest (if the calculated natural emittance exceeds the range, the objective functions will be multiplied or divided by an additional factor of more than 1), such that more and more solutions had natural emittance of about 60 pm·rad or even lower. Particularly, it was empirically found essential to evolve the population with MOPSO over enough generations (1000 generations in our study), so as to generate solutions with diverse optical parameters. Otherwise, the subsequent MOGA will quickly converge to specific local optima, with solutions gathered in a few small distinct regions in the objective function space.

In spite of the limited tuning ranges of the optimizing variables and various constraints in the optimization, after several iterations of MOPSO and MOGA, nearly continuously distributed solutions in the objective function space were obtained, showing almost a monotonic variation of the scaled ring acceptance with the natural emittance. Figure 9 shows the evolution of the population at the last iteration of MOPSO and MOGA. From the final population of MOGA, one can see a turning point around $\varepsilon_0 = 50$ pm·rad. The available ring acceptance decreases rapidly with the emittance for ε_0 below 50 pm·rad, while it decreases at a much smaller slope for ε_0 above 50 pm·rad. This suggests that for the HEPS hybrid 7BA design, it is best to keep the natural emittance above 50 pm·rad to achieve a robust nonlinear performance, i.e., with a high tolerance to small deviations in the linear optical parameters.

The PSO solutions from generation 500 to 1000 and MOGA solutions from generation 200 to 1000 in Fig. 9 were selected and re-evaluated. Among these solutions, only those with scaled ring acceptance above 2 mm^2, MA above 3% and ε_0 below 65 pm·rad were kept for post analysis. Fig. 10 shows the distributions of the selected solutions in different sub-parameter planes.

These solutions cover a horizontal integer tune range of [111, 112], which, however, is entirely different from that of the initial population (from 115 to 117, see Fig.

5). And, these solutions use stronger sextupoles than those in the initial population. Further study showed that the initial solutions with larger horizontal integer tunes were phased out with MOPSO due to their relatively smaller scaled ring acceptance. It appears that weakest possible sextupoles do not lead to the largest possible ring acceptance, and the level of sextupole strengths is neither the decisive nor exclusive factor of the nonlinear performance. In contrast, the level of the transverse focusing (reflected in the horizontal integer tune and natural chromaticities) also has a significant contribution to the available ring acceptance. In addition, it was demonstrated again that MOPSO is powerful in generating new solutions with different characteristic parameters from the existing ones. One can also see from Fig. 10 that the fractional tunes are dominant factors of the effective MA. By choosing fractional tunes at the bottom left area of the fractional tune space, one can increase the effective MA up to a maximum of about 3.8%.

As mentioned above, for HEPS it was proposed to use on-axis longitudinal injection, which has a stringent demand for MA but a less strict requirement on DA. Thus, the main goal of the nonlinear optimization is to attain as a large effective MA as possible, while keeping the effective DA large enough for on-axis injection (e.g., greater than ten times of the rms transverse beam size at the injection point). To this end, for each specific integer tune region, we did detailed numerical tracking and FMA for the solutions with the largest effective MAs, rather than those with the largest scaled ring acceptances. Several better designs were found and denoted as 'mode III', 'mode IV' and 'mode V', with the main parameters also listed in Table 1. Compared to the 'mode I'

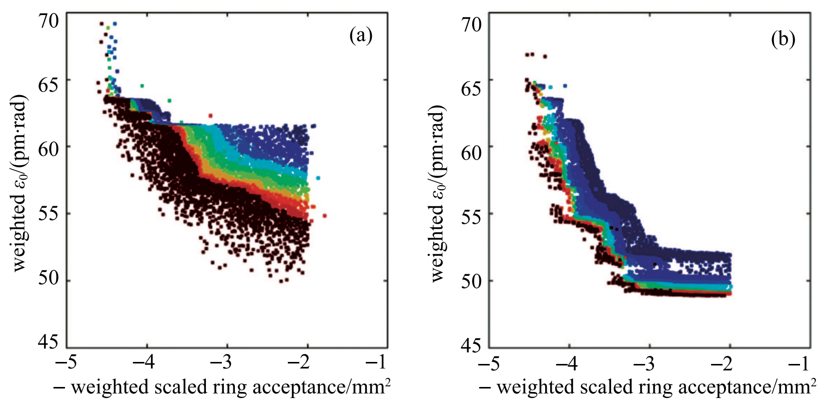

Fig. 9. (color online) Solutions of the last iteration of MOPSO (a) and MOGA (b) in the objective function space. The population is plotted at every 100th generation and marked with different colors (from blue to red).

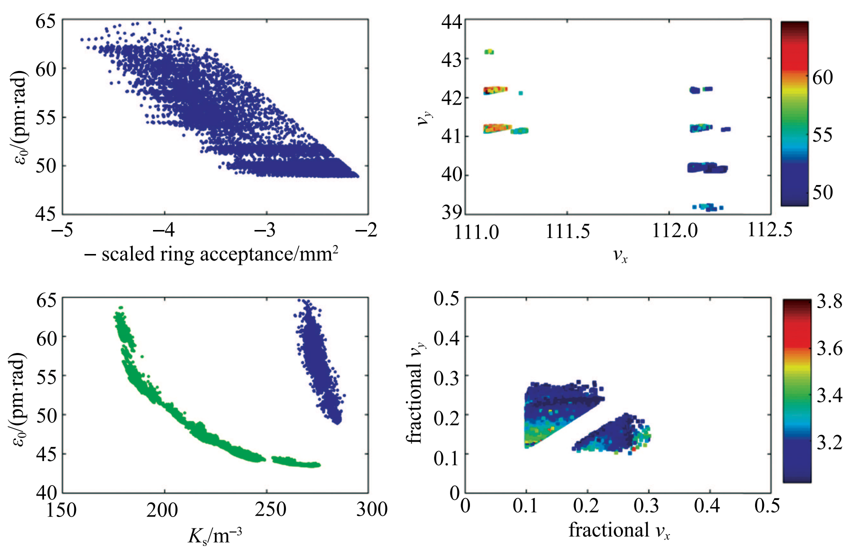

Fig. 10. (color online) Selected MOPSO and MOGA solutions projected onto different sub-parameter planes. In the upper right plot the colors represent values of the natural emittance (in unit of pm·rad), in the lower left plot the green dots represent the solutions with minimized sextupole strengths, and in the lower right plot the colors represent values of the effective MA (in unit of %).

or 'mode II' design, these designs use weaker sextupoles and octupoles, and promise lower natural emittance and larger effective DA and MA. In these designs, the fractional tunes are well separated, and all the drifts are longer than 0.1 m. As a demonstration, the effective DA and MA of the 'mode V' design are shown in Figs. 11 and 12. Note that the frequency map gets folded at y ∼ 2.5 mm. It was noted [34] that the fold corresponds to a singularity in the frequency map; after the fold, directions of fast escape may appear, causing large diffusion of trajectories. Nevertheless, a vertical acceptance of 2.5 mm is already enough for the on-axis longitudinal injection.

It is worth mentioning that in the integer tune region of (112, 40), the coupling resonance $2\upsilon_x - 2\upsilon_y = 48\times3$ is a low order structural resonance, which causes a distortion of the regular motion. Thus, although the solutions in this integer tune region promise both large MA (up to 3.8%) and ultralow emittance (close to 50 pm·rad), these were not chosen as candidate optimal designs for HEPS.

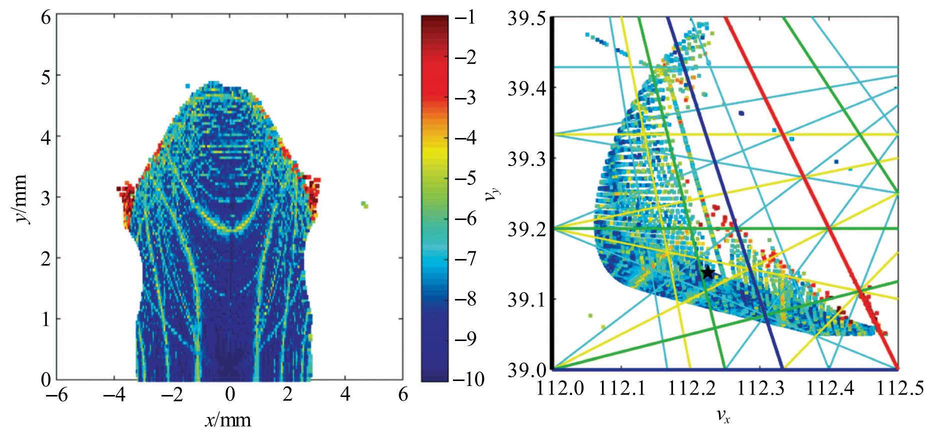

Fig. 11. (color online) Effective DA and the corresponding frequency map for the HEPS 'mode V' design.

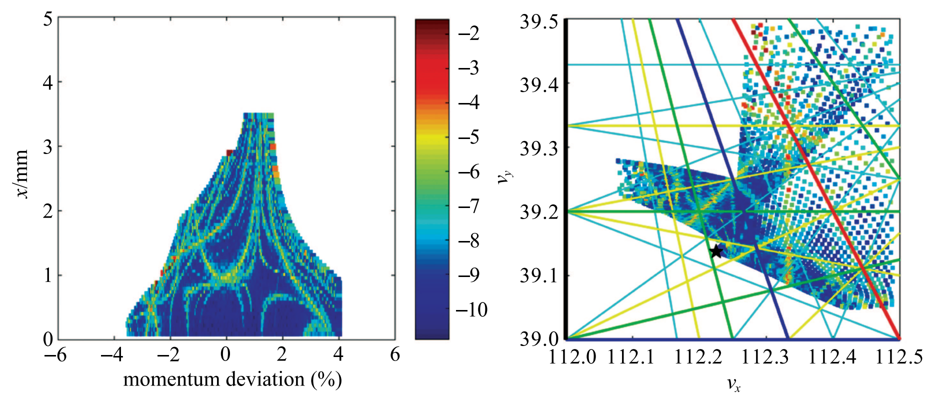

Fig. 12. (color online) Effective MA and the corresponding frequency map for the HEPS 'mode V' design.

4 Conclusion

In this paper, from an original design with a natural emittance of about 60 pm·rad, we explored the potential of the hybrid 7BA lattice design for the HEPS project, with a successive and iterative implementation of the MOPSO and MOGA. It turns out that with the hybrid 7BA lattice, it is feasible for HEPS to achieve a sufficient ring acceptance for beam accumulation with on-axis longitudinal injection, and simultaneously reduce the natural emittance to about 50 pm·rad.

In this study, we also investigated the relations between nonlinear performance and linear optics. It was found that there is neither a decisive nor exclusive factor of the nonlinear performance. In contrast, to simultaneously attain an ultralow emittance and the largest possible ring acceptance, it needs to reach a balance among various factors, especially the sextupole strengths and the integer and fractional tunes.

In addition, we showed an effective way to explore the potential of a MBA lattice from a specific design, while not necessarily requiring a deep understanding of the physics behind the lattice design and the complicated relations between the nonlinear dynamics and linear optics. The key point is to evolve a large enough population with MOPSO and MOGA in a successive and iterative way. As demonstrated, MOPSO has an intrinsic ability to breed more diversity in the population during evolution, and once there is enough diversity in the population, MOGA can reach better convergence than MOPSO. Thus, combining MOPSO and MOGA in the optimization will be effective and powerful in approaching the global optima, regardless of whether or not enough diversity is seeded in the initial population. It is believed that such an optimization procedure can benefit other DLSR designs with the same or similar objective functions (e.g., using DA and MA in presence of magnetic errors instead of the effective DA and MA, or using Touschek lifetime instead of MA), and can be generalized to other explorative multi-objective optimization problems.

References

1 Z. Zhao, Reviews of Accelerator Science and Technology, **3**: 57 (2010)
2 D. Einfeld, J. Schaper, and M. Plesko, in *Proceeding of PAC'95 (Dallas, USA, 1995)*, p. 177–179
3 R. Hettel, J. Synchrotron Radiat., **21**: 843–855 (2014)
4 E. Al-Dmour et al, J. Synchrotron Radiat., **21**: 878–883 (2014)
5 M. Johansson et al, J. Synchrotron Radiat., **21**: 884–903 (2014)
6 P. F. Tavares et al, J. Synchrotron Radiat., **21**: 862–877 (2014)
7 L. Liu et al, J. Synchrotron Radiat., **21**: 904–911 (2014)
8 Y. Jiao, Y. Cai, and A. W. Chao, Phys. Rev. ST Accel. Beams, **14**: 054002 (2011)
9 L. C. Teng, Fermilab Report No. TM-1269, 1984
10 Y. Cai, K. Bane, R. Hettel, Y. Nosochkov, M.H. Wang, and M. Borland, Phys. Rev. ST Accel. Beams, **15**: 054002 (2012)
11 Y. Jiao and G. Xu, Chin. Phys. C, **37**: 117005 (2013)
12 M. Borland et al, J. Synchrotron Radiat., **21**: 912-936 (2014)
13 Y. Jiao and G. Xu, Chin. Phys. C, **39**: 067004 (2015)
14 L. Farvacque et al, in *Proceeding of IPAC2013 (Shanghai, China, 2013)*, p. 79–81
15 M. Borland et al, in *Proceeding of IPAC2015 (Richmond, USA, 2015)*, p. 1776–1778
16 G. Xu, Y. Jiao, and Y.M. Peng, Chin. Phys. C, **40**: 027001 (2016)
17 F. Willeke, in *Proceeding of IPAC2015 (Richmond, USA, 2015)*, p. 11–16
18 Y. Jiao and Z. Duan, Nucl. Instrum. Methods Phys. Res., Sect. A, **841**: 97–103 (2017)
19 A. Terebilo, SLAC-PUB-8732, 2001
20 L. Nadolski and J. Laskar, Phys. Rev. ST Accel. Beams, **6**: 114801 (2003)
21 G. Xu et al, in *Proceeding of IPAC2016 (Busan, Korea, 2016)*, WEOAA02
22 M. Aiba, M. Böge, F. Marcellini, Á. Saá Hernández, and A. Streun, Phys. Rev. ST Accel. Beams, **18**: 020701 (2015)
23 Y. Jiao, Chin. Phys. C, **40**: 077002 (2016)
24 I. V. Bazarov and C.K. Sinclair, Phys. Rev. ST Accel. Beams, **8**: 034202 (2005)
25 L. Yang et al, Nucl. Instrum. Methods Phys. Res., Sect. A, **609**: 50–57 (2009)
26 M. Borland et al, in *Proceeding of PAC'09 (Vancouver, Canada, 2009)*, p. 3850–3852
27 L. Yang, Y. Li, W. Guo, and S. Krinsky, Phys. Rev. ST Accel. Beams, **14**: 054001 (2011)
28 W. Gao, L. Wang, and W. Li, Phys. Rev. ST Accel. Beams, **14**: 094001 (2011)
29 Z. Bai, L. Wang, and W. Li, in *Proceeding of IPAC2011 (San Sebastián, Spain, 2011)*, p. 2271–2273
30 X. Pang and L.J. Rybarcyk, Nucl. Instrum. Methods Phys. Res., Sect. A, **741**: 124–129 (2014)
31 X. Huang and J. Safranek, Nucl. Instrum. Methods Phys. Res., Sect. A, **757**: 48–53 (2014)
32 K. Deb, IEEE Trans. Evol. Comput., **6**: 182 (2002)
33 S. K. Tian, HEPS internal report, 2016
34 J. Laskar, in *Proceeding of PAC'03 (Portland, USA, 2003)*, p. 378–382